Acta Astronautica 111 (2015) 308–316

Contents lists available at ScienceDirect

Acta Astronautica

journal homepage: www.elsevier.com/locate/actaastro

Numerical exploration of dissimilar supersonic coaxial jets mixing

Malsur Dharavath, P. Manna, Debasis Chakraborty *

Directorate of Computational Dynamics, Defence Research and Development Laboratory, Hyderabad 500058, India

ARTICLE INFO

Article history:
Received 18 September 2014
Received in revised form
18 February 2015
Accepted 2 March 2015
Available online 10 March 2015

Keywords:
CFD
Convective Mach number
Dissimilar gases

ABSTRACT

Mixing of two coaxial supersonic dissimilar gases in free jet environment is numerically explored. Three dimensional RANS equations with a k–ε turbulence model are solved using commercial CFD software. Two important experimental cases (RELIEF experiments) representing compressible mixing flow phenomenon under scramjet operating conditions for which detail profiles of thermochemical variables are available are taken as validation cases. Two different convective Mach numbers 0.16 and 0.70 are considered for simulations. The computed growth rate, pitot pressure and mass fraction profiles for both these cases match extremely well with experimental values and results of other high fidelity numerical results both in far field and near field regions. For higher convective Mach number predicted growth rate matches nicely with empirical Dimotakis curve; whereas for lower convective Mach number, predicted growth rate is higher. It is shown that well resolved RANS calculation can capture the mixing of two supersonic dissimilar gases better than high fidelity LES calculations.

1. Introduction

The supersonic combustion ramjet (scramjet) offers potentially cheaper alternative for high Mach number flight to space as well as for military applications and is the preferred choice for air-breathing engine in hypersonic flight. Establishing an efficient supersonic combustion process over a wide range of flight Mach numbers still remains a challenging process. The fuel injection system and combustor geometry must simultaneously provide sufficient fuel–air mixing and minimal losses. Computational fluid dynamics (CFD) codes based on the Reynolds averaged Navier–Stokes (RANS) equations are extensively used in the development of high speed air breathing engines. The maturation of multipurpose CFD codes coupled with advancements in computer architectures has substantially reduced the turnaround time required to perform steady-state Reynolds-averaged simulations. Turbulence models employed in these codes employ many adhoc assumptions and empirically determined coefficients. So to make CFD methods a reliable tool and to apply with confidence in the design exercise, it needs to be validated against reliable experimental results that are representative of compressible mixing flow phenomenon encountered in scramjet combustors.

In the past, experimental studies of high speed mixing flows mostly focused on two stream planar mixing layers mainly to gain understanding on the effect of compressibility on mixing. For high speed flows, it is seen that slight variations in the mixing rate predictions resulting in large discrepancies in combustor performance. Dimotakis [1] reviews much of these literatures present in two stream planar mixing layers. However, the two stream planar mixing layers contain relatively small regions of high speed propulsion flows; while the mixing between partially mixed fuel–air plumes and fresh air ingested by engine intake occurs in the greater part of a high speed air breathing engine.

Gutmark et al. [2] considered the effects of convective Mach number on the mixing of circular, rectangular, and elliptical supersonic jets of various gases in a supersonic coflow of air. Rossman et al. [3] were consistent with findings on the effects of compressibility on mixing-layer growth rate such

* Corresponding author. Tel.: +91 40 24583310; fax: +91 40 24340037.
E-mail address: debasis_cfd@drdl.drdo.in (D. Chakraborty).

http://dx.doi.org/10.1016/j.actaastro.2015.03.001
0094-5765/

as the equation of Dimotakis [1]. He also found the ratio of compressible mixing-layer growth to incompressible mixing-layer growth rate as a function of convective Mach number (M_c), for the He–O_2 and the measured Argon growth rate with experiment. Carty [4] developed and validated a supersonic Helium–Air coannular jet facility. However, sufficient details could not be found for this experiment for code-validation purposes. Experimental studies of mixing of two coaxial supersonic streams (outer jet of air and an inner jet of either a Helium–oxygen mixture or pure Argon) in free jet environment carried out by Cutler et al. [5–7] generated important profiles for different flow parameters which are very useful for CFD validation studies. The streamwise development of the flow in the experimental condition is dominated by turbulent stresses instead of pressure forces, and calculations are sensitive to proper turbulence modeling. The two stream mixing layer which is formed between the center jet and the coflow near the nozzle exit depends on the injectants for shear and the compressibility of the mixing layer. The Helium condition is pressure matched at the nozzle exit resulting in a high convective Mach number of 0.7 representing the flow in scramjet combustor. The Argon condition, on the other hand, was both pressure and velocity matched which produced a mixing layer with a convective Mach number of 0.16. Free jet features of the flows provide easy access for both optical instrumentation and probes for detailed flow investigations. Being axisymmetric, a minimum number of experimental measurements are required to fully characterize the flow. The experiment contains comprehensive set of measurements including pitot pressure, mean and rms velocities, and gas sampling. The model geometry, flow conditions, and measurement uncertainties were all well documented, resulting in a package that was well suited for model validation efforts. Because of these attractive features of this experiment, it was adopted by a working group of the NATO Research and Technology Organization as a test case for their CFD development and validation activity.

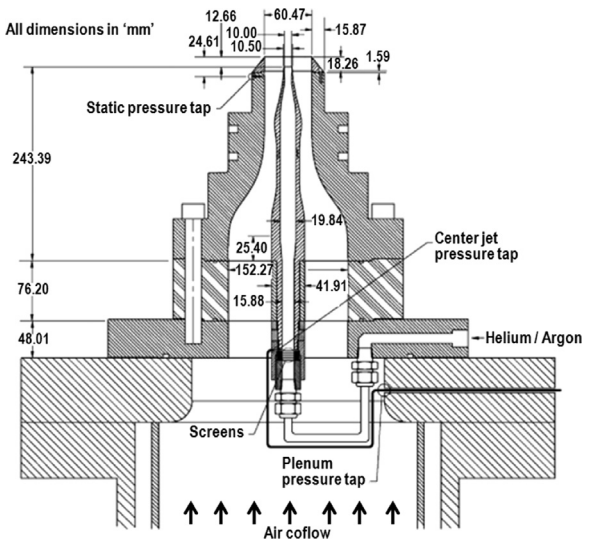

Fig. 1. Coaxial jet-nozzle assembly (reproduced from Ref. [9]).

Number of CFD studies [5,7,8–11] with different level of turbulence modelings starting from two equation turbulence models [9,10] to more advanced LES model [11] were reported in the literature for this experimental condition in last few years. RANS calculations employing structured finite difference code VULCAN [12] along with the k–ω turbulence model [13] showed non-physical discontinuities in slope of mole fraction and pitot pressure which were attributed to inadequacies in the turbulence model. Baurle and Edwards [11] adopted hybrid RANS/LES approach over RANS calculation as the latter is shown to depend heavily on the modeled turbulent transport of heat and mass transfer. LES results of Baurle and Edwards [11] are shown to be no more predictive than the baseline Reynolds-averaged predictions. Moreover, LES approach for engineering applications is very costly in terms of computing resource. It is clear that supersonic mixing of coaxial nonreating jets requires further studies to have better predictive capabilities and the search for a reliable numerical tool for solving the engineering problems of high speed air breathing propulsion is still continuing. Supersonic mixing layer of two dissimilar gases, although geometrically simple, represents canonically the physical process of mixing under compressible condition similar to scramjet combustor. In this paper, experimental condition of nonreacting mixing of two coaxial supersonic streams is numerically explored by using a commercial CFD software [14] and results were

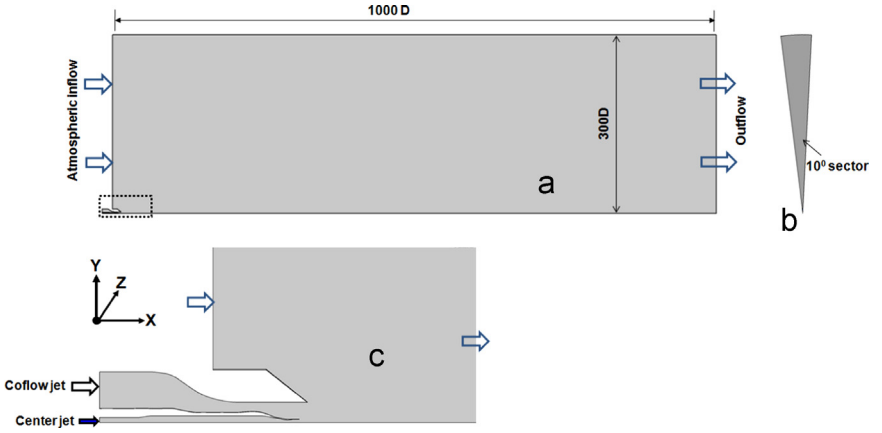

Fig. 2. Computational domain with boundary details, (a) front view, (b) side view and (c) blown up view near the nozzle.

analysed and compared with experimental data as well as with other numerical calculations.

2. Experimental facility for which computations are carried out.

The experimental test facility for which the computations are carried out is explained in detail in the literature [9,10]. The relevant features of the geometry and flow conditions are explained in this section. The schematic of coaxial jet assembly which was tested in transverse jet facility [15] at NASA Langley Research center is taken from Ref. [10] and reproduced in Fig. 1. The axisymmetric center body contains a supersonic nozzle for the primary Argon/Helium jet, and the gap between the center and outer bodies creates a supersonic nozzle for the concentric coflow secondary air jet. Both nozzles were designed to provide a nominal Mach number of 1.8 at the exit. Screens were installed near the entrance of the center body to make the primary stream uniform and to lower turbulence. Three pressure taps (downstream of the screens, coflow body and facility plenum) are located in the nozzle assembly. Thermocouples are positioned in the gas supply lines. Air is provided to the facility from a central air station, and the He–O_2 mixture/Argon is provided to the center body from a bottle trailer containing premixed gas. Visualization of the flow is done through conventional schlieren and shadowgraph and pitot, gas-sampling, and total-temperature probes were employed to measure various flow parameters. Oxygen flow-tagging technique (RELIEF) velocity-measurement technique [16] was used to obtain distributions of mean and fluctuating axial component velocity. Uncertainties in measurements are due to both facility unsteadiness and variations in set point and to transducer error which are quantified in Ref. [9] and [10]. A mixture of 5% oxygen and 95% Helium by volume is used for Helium–oxygen mixture. The presence of oxygen in the center jet enabled the use of RELIEF technique to obtain non-intrusive velocity measurements. The exit flow pressure for both coflow and center-jet nozzles is 1 atm. Although, both jets are at Mach 1.8 but because of the greater speed of sound of the center jet, its velocity is more than twice that of the coflow.

3. The code and Computational details

Present simulation uses commercial CFD software CFX 11 [14] which is three dimensional finite volume Reynolds Averaged Navier Stokes (RANS) solver on structured or unstructured grid. The solver provides option to use different turbulence models namely, k–ε, RNG k–ε, k–ω or SST turbulence model. The software has three major modules, (i) *preprocessor* – import grids from a grid generator and set up the boundary condition, select turbulence model and initialize flow field (ii) *solver manager* – solves the flow field based on the grid and the boundary condition and (iii) *postprocessor* – helps in visualizing flow field data. The solver

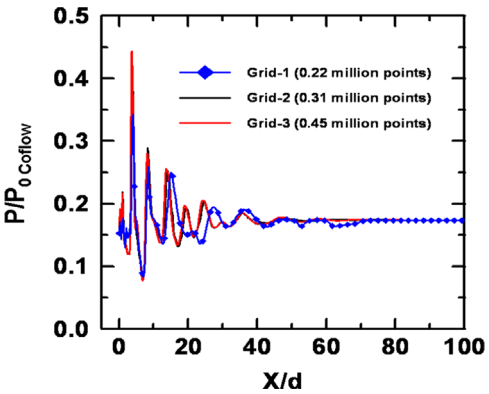

Fig. 4. Centerline pressure distribution with three different grid.

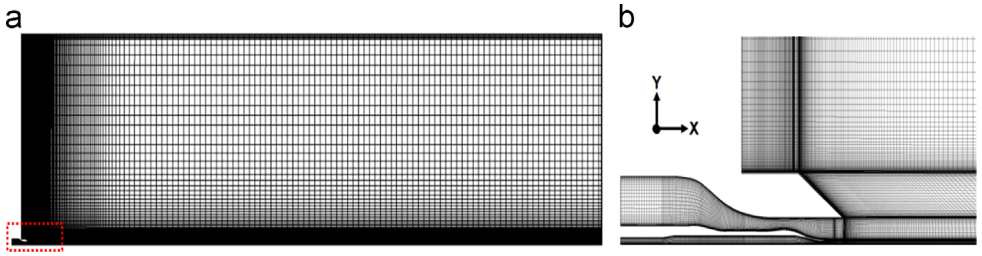

Fig. 3. Grid distribution on various regions (total grid size ~0.45 millions points), (a) symmetry plane and (b) extracted view at nozzle region.

Table 1
Inflow parameters for the two test cases (1) Argon–Air (2) He–O_2 mixture and Air.

Parameters	Case-1:Argon–Air			Case-2: He–O_2 mixture and Air		
	Ar jet	Air jet	Ambient	He–O_2 jet	Air jet	Ambient
Mach no.	1.8	1.8	0.025	1.81	1.8	0.025
Total temp.(T_0)(K)	298	294	294	305	300	294
Total Pr.(P_0) (MPa)	0.616	0.581	0.101	0.615	0.58	0.101
Exit momentum at nozzle (N)	42.92	1462	–	42.82	1462	–
Exit pressure at nozzle (MPa)	0.075	0.112	–	0.077	0.112	–

has different schemes for solving the advection term. For high speed flows, high resolution schemes are preferred for better accuracy and robustness. To find out the accuracy and the range of applications, the software has been validated for various complex aerospace problems including staged sonic injection in supersonic flow inside rectangular duct [17], supersonic base flow [18], free stream and rocket exhaust interaction [19], transverse sonic injection in supersonic stream [20], supersonic jet impingement problem in an inclined plate [21], hypersonic air intake problem [22], missile movement in canister [23] etc. and obtained very good match with experimental and flight measured values.

3.1. Numerical scheme

The high resolution scheme used in the simulation is explained in Ref. [23]. In the solver, finite volume is created around the integration point by connecting the neighboring nodes. Solution fields and other properties are stored at the nodes. However, to evaluate many of the terms, the solution field or solution gradients must be approximated at the integration point. The advection term in the solver is modeled by exprressing the finite element shape function φ at integration point in terms of nodal values of φ and is cast in the form $\varphi_{ip} = \varphi_{up} + \beta \nabla\varphi.\Delta\vec{r}$: where, φ_{up} is the value at the upwind node and φ_{ip} is the value at the integration point. The high resolution scheme is a special non-linear recipe for β at each node computed to be as close to 1 as possible without intrroducing new extrema. The advective flux is then evaluated using the values of β and $\nabla\varphi$ at upwind point. The recipe for β is based on boundedness principle used by Barth and Jespersen [24] which utilizes a multi-dimensional monotone reconstruction of cell averaged data and Roe's flux function. This differs from the other upwind schemes for unstructured meshes which do not perform reconstructions of cell averaged data. This methodology involves first computing a φ_{min} and φ_{max} at each node using a stencil involving adjacent nodes (including the node itself). Next, for each integration point around the node, equation for the nodal value is solved for β to ensure that it does not undershoot φ_{min} and overshoot φ_{max}. The nodal values of β are taken to be minimum of all integration point values surrounding the nodes. The values of β is also not allowed to exceed 1. This algorithm is shown to be Total Variation Diminishing (TVD) in one dimension. The present simulation uses the k–ε turbulence model [25].

4. Results and discussions:

Taking the advantage of the symmetry of the flow field only 10° sector is simulated. The computational domain is shown in Fig. 2 where the outflow and radial boundaries are extended up to 1000 D and 300 D respectively (D=10 mm being the diameter of the central jet). A fine structured mesh of 0.45 million size involving $387 \times 81 \times 13$ distribution is generated in computational domain. The grid distribution in the computational domain along with the blown up view near the nozzle exit is shown in Fig. 3. Inflow flow variables (Mach number, Total pressure (P_0) and Total Temperature (T_0)) used for the computations for two test cases, namely the mixing of (1) Argon–Air and (2) Helium–oxygen mixture and air are tabulated in Table 1. The ambient air flow (M=0.025) caused due to the entrainment action of the jet is also considered in the simulation. The nozzle exit momentum of the outer air jet is 1462 N whereas the momentum of the inner jets of Argon and He–Air mixture is about 43 N. The nozzle exit pressures for the two test conditions are also provided in Table 1. Chamber total pressure (P_0) and total temperature (T_0) condition is imposed at inflow plane and subsonic outflow condition with atmospheric pressure was implemented at the outlet plane. No slip, adiabatic wall condition is imposed on all walls. Scalable wall function due to Menter et al. [26] is used in the nozzle walls of the coflow jet and the center jet. To trigger the turbulence activity in the flow field quickly, turbulence intensity and viscosity ratio (μ_t/μ_l) at inflow plane is set as 5% and 10 respectively. However, the flow parameters downstream are independent on these inflow turbulence parameters. These observations are consistent with the studies of many researchers [27–29], where they found that attainment of self similar state of jets and mixing layers are not

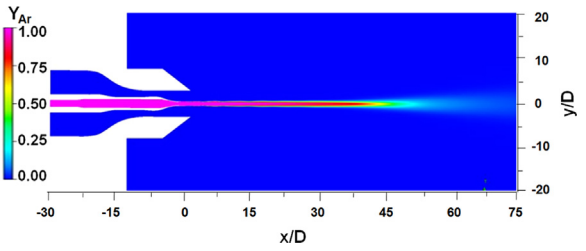

Fig. 6. Argon mass fraction distribution in the symmetry plane.

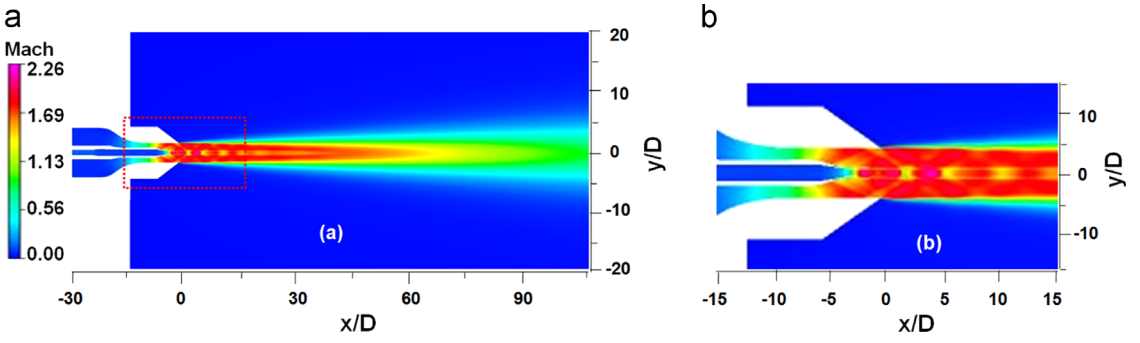

Fig. 5. Mach number distribution in (a) symmetry plane (b) blown up view near the exit.

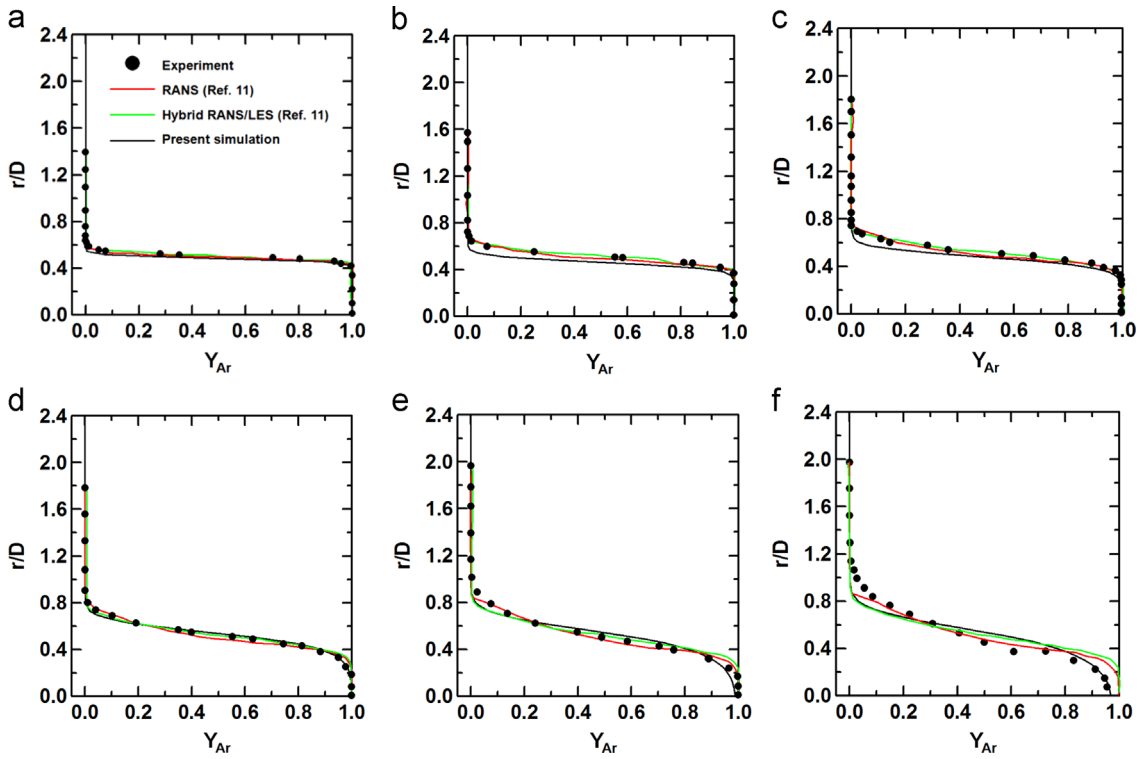

Fig. 7. Comparison of computed Argon mass fraction profile with experimental result, RANS and LES calculation (Ref. [11]) at (a) $x/D=0.99$ (b) $x/D=4.2926$, (c) $x/D=8.1102$, (d) $x/D=12.1381$, (e) $x/D=18.1$ and (f) $x/D=22.04$.

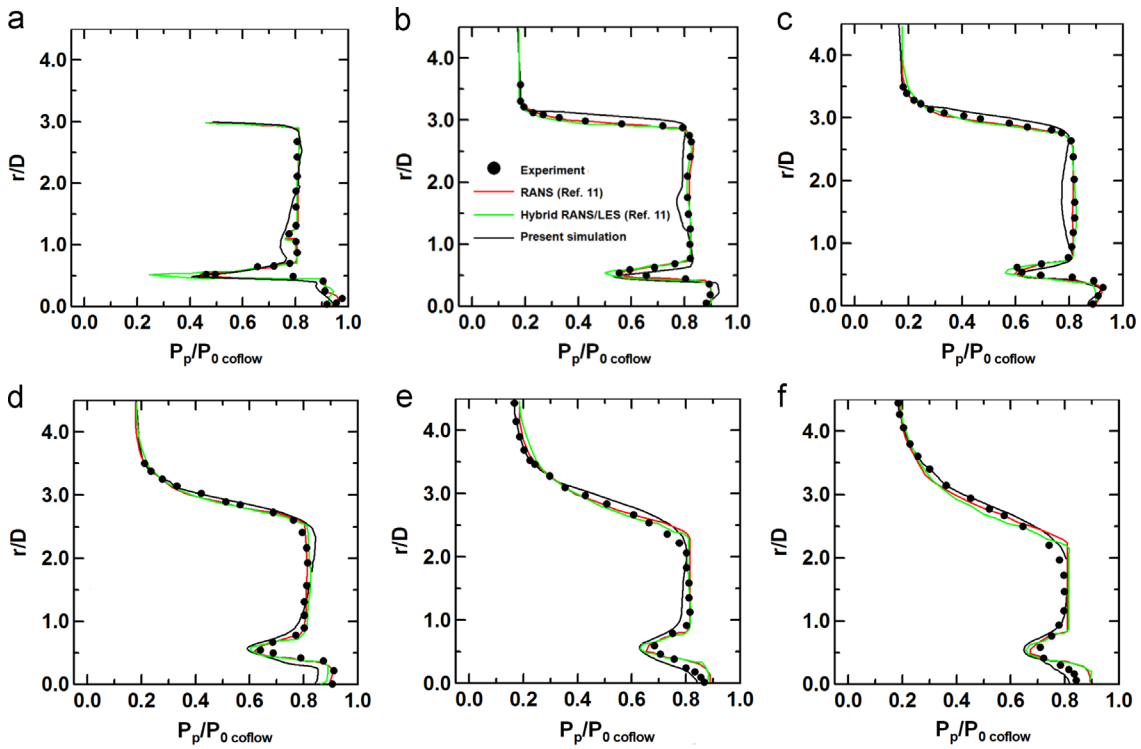

Fig. 8. Comparison of computed pitot pressure profile with experimental result, RANS and LES calculation (Ref. [11]) at (a) $x/D=0.99$ (b) $x/D=4.2926$, (c) $x/D=8.1102$, (d) $x/D=12.1381$, (e) $x/D=18.1$ and (f) $x/D=22.04$.

dependent of initial values of turbulent intensities or forcing. Physical time step of 10^{-5} is adopted in the simulation. Steady state of the solution is achieved by checking the maximum values of log-normalized residue (which is four order less for various flow variables) and global mass, momentum, and energy imbalance ($<0.1\%$ between outlet and inlet of the computational domain).

4.1. Argon–Air results

To check the grid independence of the results simulations are carried out with three different grids namely 0.22, 0.31 and 0.45 million points and the nondimensionalised centerline pressure distribution ($P/P_{0\ \mathrm{coflow}}$) ($P_{0\ \mathrm{coflow}}$ is the total pressure of the coflowing stream) is compared in Fig. 4. A close match of the pressure data between the three levels of grid demonstrates the grid convergence of the results. Mach number distribution in the symmetry plane (with blown up view near the nozzle exit) is shown in Fig. 5. It can be observed that all the fine features of the flow field including number of shock cells are crisply captured in the simulation. The mass fraction distribution of Argon gas in the symmetry plane is shown in Fig. 6. Due to high momentum of coflowing compared to Argon jet, the diffusion of Argon gas in air stream is very little. The comparison Argon gas mass fraction profile at $x/D=0.99$, 4.2926, 8.1102, 12.1381, 18.11 and 22.03 between experimental data, RANS data of Vulcan and LES data [11] are compared in Fig. 7. Present computations show a very good match with the experimental results at near field as well as in the far field locations. If we closely look the profiles at $x/D=22.03$ (Fig. 7(f)), we can observe that in the central zone ($0<r/D<0.4$), present computations match the experimental value better than the VULCAN results and LES results. The experimental pitot pressure profile is compared with computation values in Fig. 8 at $x/D=0.99$, 4.2926, 8.1102, 12.1381, 18.11 and 22.03 and very good match is obtained. It is clear that well resolved RANS calculation can predict the mean profiles of supersonic mixing layers as good as LES.

The mixing layer boundaries (mole fraction of Argon gas between 0.01 and 0.99) obtained from the numerical simulation and are compared with RANS results of VULCAN (Ref. [9] and [10]) and are shown in Fig. 9. Although the lower boundary of Argon layer ($\delta_{0.99}$), match extremely well between these two computations, present computation over predicts the upper boundary of Argon ($\delta_{0.01}$) in the region $10<x/D<22$ by 10–15%. The cause of this difference was not explored in detail which is conjectured to be due to difference in grid structure, numerical scheme and turbulence model in two computations. The thickness of the mixing layer between the center jet and coflow is defined as $\delta_{0.01}$–$\delta_{0.99}$. The rate of change of this thickness, or mixing-layer growth rate, is 0.0432.

The nondimensionalised velocity profiles (u/u_e) (u_e being the free stream central jet velocity) at various axial locations $x/D=0.99$, 4.29, 8.11, 112.13, 18.10 and 22.04 are plotted against nondimensionalised distance (y/δ) in Fig. 10. We can observe that the velocity profiles have collapsed into single curve indicating the attainment of self similarity at $x/D=4.3$.

4.2. Helium oxygen (He–O_2) mixture–Air results

The comparison of Helium gas mass fraction profile at $x/D=0.99$, 4.29, 8.11, 12.14, 18.1 22.04 between experimental data, RANS data of Vulcan and LES data [11] are

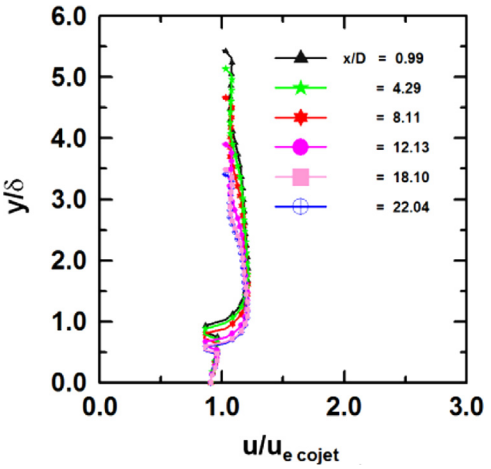

Fig. 10. Nondimesionalised velocity profile at various axial locations.

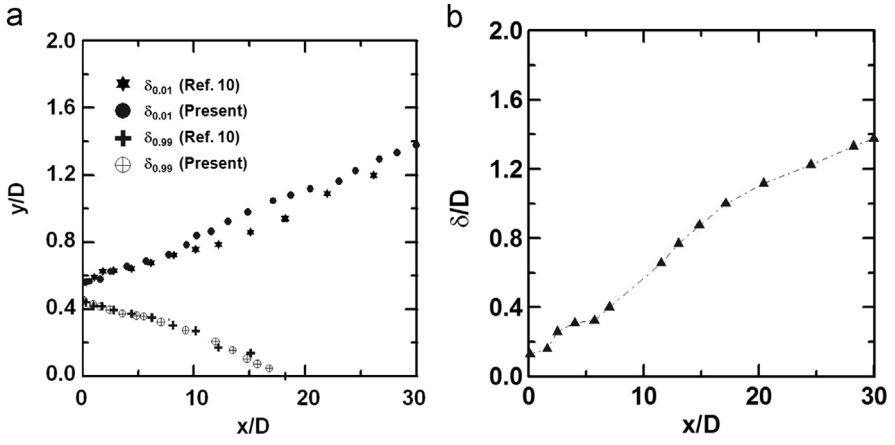

Fig. 9. (a) Mixing region boundaries and (b) mixing layer thickness for Ar–Air case.

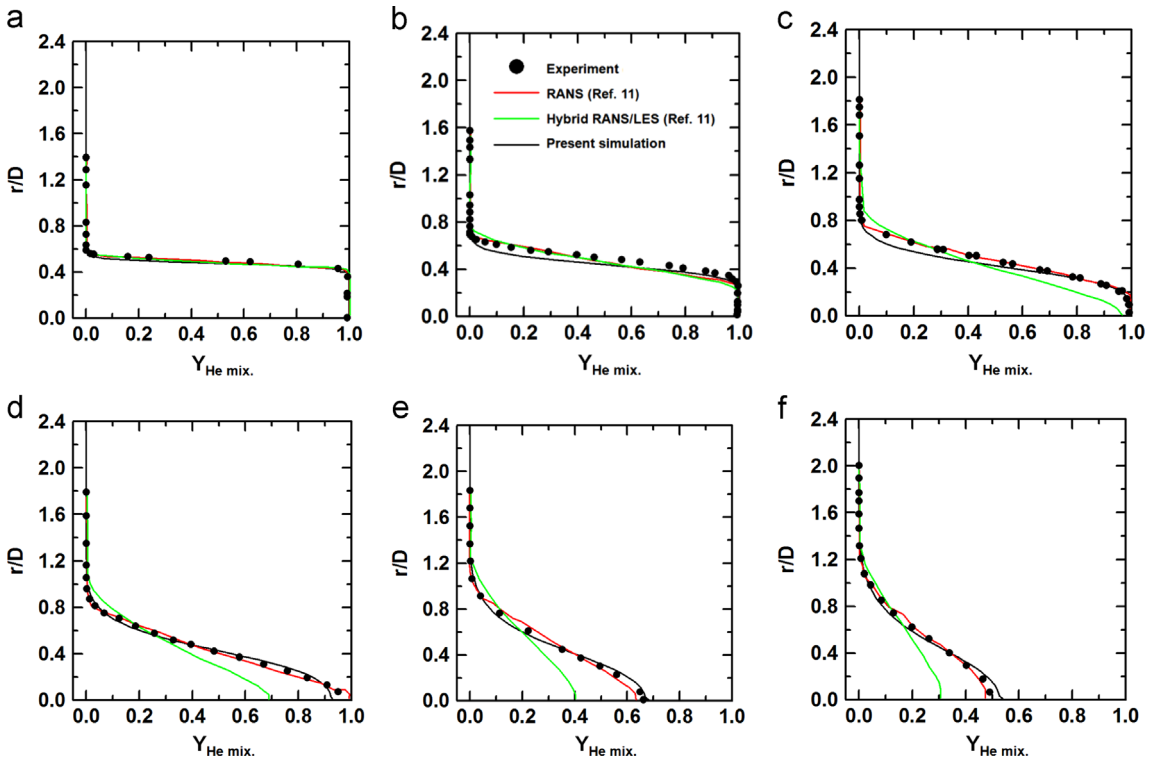

Fig. 11. Comparison of Helium mass fraction profile between experimental result, RANS, LES (Ref. [11]) and present computations at $x/D=0.99$, 4.2926, 8.11, 12.14, 18.11 and 22.04.

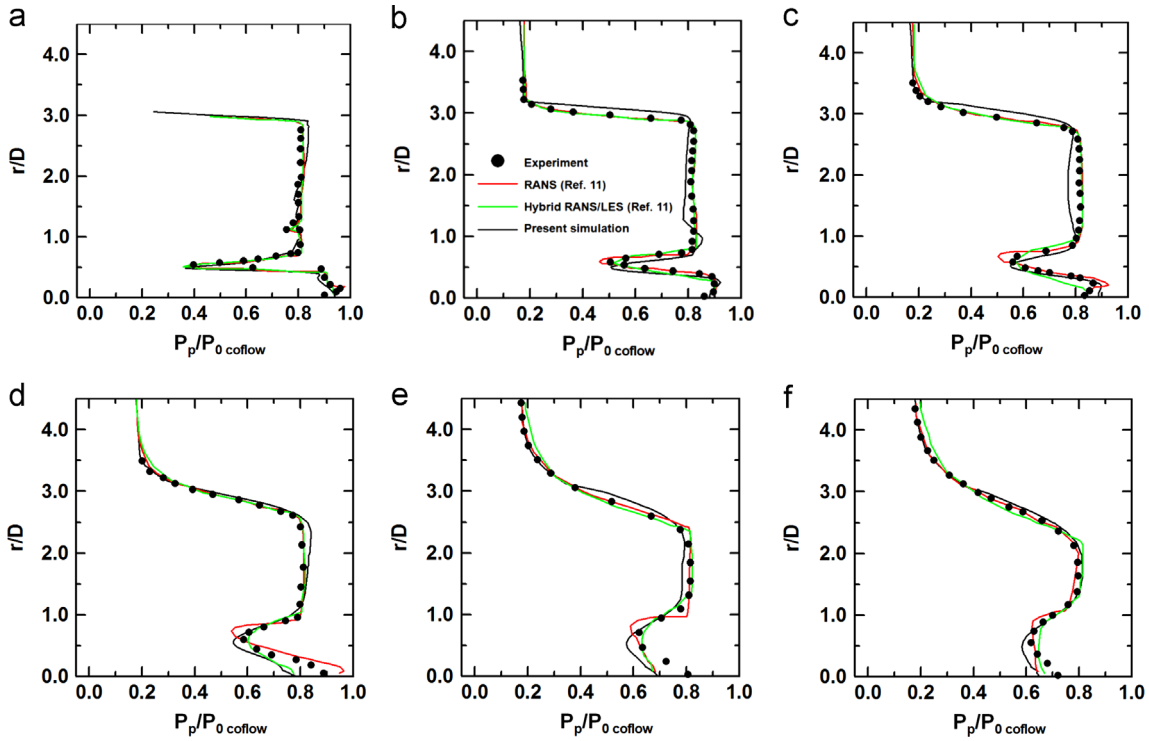

Fig. 12. Comparison of pitot pressure profiles for He–O_2–Air mixing layer between experimental result, RANS, LES (Ref. [11]) and present computation at $x/D=0.99$ 4.2926, 8.1102, 12.1381, 18.11 and 22.04.

compared in Fig. 11. Present computations show a very good match with the experimental results at near field as well as far field. The experimental pitot pressure profile is compared with RANS, Hybrid RANS/LES and present computations at $x/D=0.99$, 4.29, 8.11, 12.14, 18.11 and 22.04 in Fig. 12. Although RANS results (Ref. [11]) and present computations match very well with experimental data at both far field and near field regions, hybrid RANS / LES computations failed to capture the pressure profile towards inner jet for $x/D>4.29$. The computed total temperature profile at $x/D=10.06$ is compared with experimental results and RANS results in Fig. 13. A very good match of computations and experimental data is observed. For $y/D>0.7$, both the computations slightly over predict ($\sim$1%) the experimental value. The computed He–O_2/Air mixing layer boundaries are compared with RANS results of VULCAN (Ref. [9]) in Fig. 14. A good overall match is obtained and the computed mixing layer thickness is 0.0562. The computed nondimensionalised growth rate is compared with RANS calculation (Ref. [9]) as well as Dimotakis fit (Ref. [1]) in Fig. 15. The mixing layer growth rate (δ) is nondimensionalised with incompressible growth rate (δ_{inc}) defined as (Ref. [10]):

$$\delta_{inc}=0.17*\frac{\left[1-\frac{u_2}{u_1}\right]*\left[1+\left(\frac{\rho_2}{\rho_1}\right)^{0.5}\right]}{1+\frac{u_2}{u_1}\left(\frac{\rho_2}{\rho_1}\right)^{0.5}}$$

where u_1, u_2, ρ_1, ρ_2 are the velocities and densities of inner and outer streams respectively. For both the cases, computed growth rate matches with RANS calculations. Although for He–O_2/Air mixing computed growth rate matches nicely with Dimotakis curve, but for Argon–Air mixing ($M_c=0.16$), the computed growth rate is more than Dimotakis curve by 30%.

5. Conclusion

Three dimensional RANS simulations with the k–ε turbulence model are presented to study the mixing of coaxial supersonic streams of dissimilar gases in a free jet environment. Two important experiments namely mixing of (1) Argon/Air streams and (2) He–O_2 (95% He and 5%

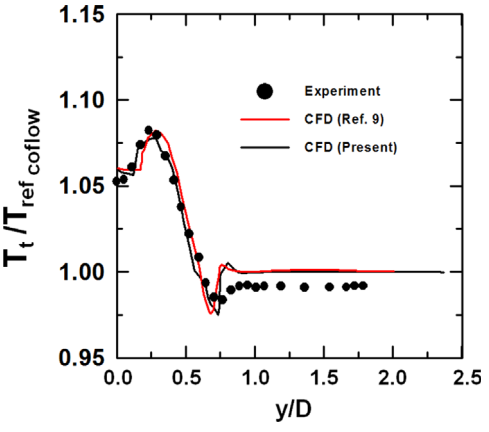

Fig. 13. Comparison of total temperature (T_t) measurements with RANS data (present computation and VULCAN (Ref. [9])) at $x/D=10.06$.

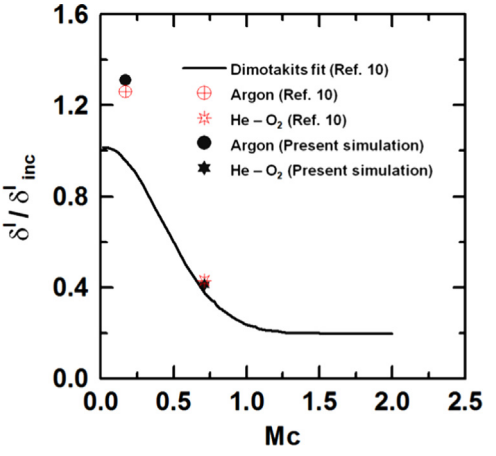

Fig. 15. Comparison of nondimensionalised growth rate Vs Convective Mach number.

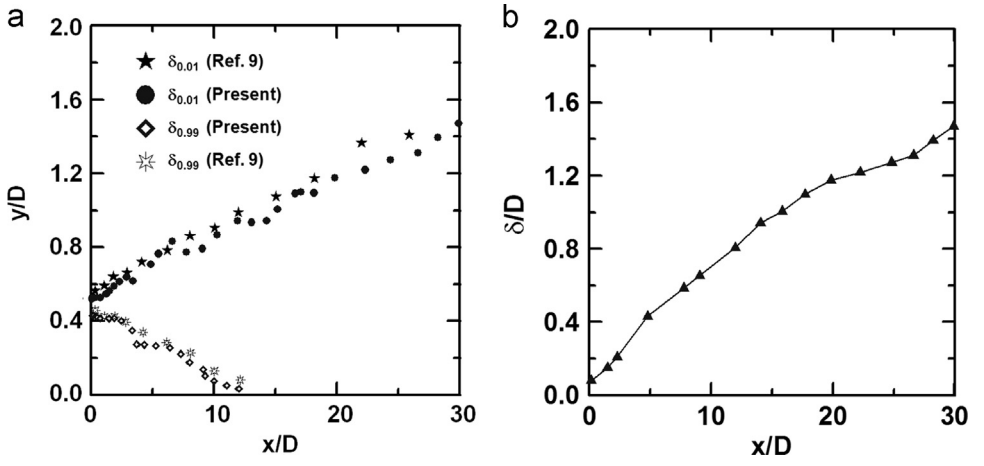

Fig. 14. (a) Mixing region boundaries and (b) mixing layer thickness for He–O_2–Air case.

oxygen) mixture/Air streams representing compressible mixing flow phenomenon under scramjet operating conditions are numerically explored. The convective Mach number (M_c) of Argon/Air case is 0.15 whereas that of He–O_2 mixture/Air case is 0.7. Although, both jets are at Mach 1.8 but because of the greater speed of sound of the center jet, its velocity is more than twice that of the outer stream. A fine structured mesh involving 0.45 million grid points are utilized in the computational domain and the simulations captured all pertinent flow features including number of shock cells near the exit planes. The species mass fraction and pitot profiles at various axial locations-match very well with experimental data as well as calculations of other numerical results (VULCAN) and LES for far field and near field regions. For Argon/Air case, present computations match the profile better with experimental data compared to VULCAN and LES results at far field region. For He–O_2/Air mixing case, although both present computation and VULCAN results compare the experimental data well for all the axial location, hybrid RANS/LES method fails to capture the experimental trend of the inner jet particularly at far field region ($x/D > 4.29$). A good overall match is obtained the mixing layer boundaries between the VULCAN results and present computations for both the cases, present computation over predicts the upper boundary of Argon ($\delta_{0.01}$) in the region $10 < x/D < 22$ by 10–15%. The nondimensionalised growth rate for He–O_2/Air mixture ($M_c = 0.7$) matches well with the empirical Dimotakis curve, while the computed growth rate of Argon/Air mixture is higher than that of Dimotakis relation. The present simulations has indicated that well resolved RANS calculation can capture adequately the time averaged flow profiles of supersonic mixing layer.

References

[1] P.E. Dimotakis, Turbulent Free Shear Layer Mixing and Combustion, in: S.N.B. Murthy, E.T. Curran (Eds.), High-Speed Flight Propulsion Systems (Progress in Astronautics and Aeronautics), 137, AIAA, Washington, DC, 1991, pp. 265–340.

[2] E. Gutmark, K.C. Schadow, K.J. Wilson, Effect of convective Mach number on mixing of coaxial circular and rectangular jets, Phys. Fluids A 3 (1) (1991) 29–36.

[3] T. Rossman, M. Mungal, R. Hanson, A new shock tunnel facility for high compressibility mixing layer studies, in: Proceedings of the 37th Aerospace Sciences Meeting and Exhibit, Reno, NV, Paper no. AIAA 99-0415, January 11–14, 1999.

[4] A.A. Carty M.S. thesis, Development and Validation of a Supersonic Helium–Air Coannular Jet Facility, The George Washington University, 1998 School of Engineering and Applied Sciences.

[5] A.D. Cutler, A.A. Carty, S.E. Doerner, G.S. Diskin, J.P. Drummond, Supersonic coaxial jet flow experiment for CFD Code validation, in: Proceedings of the 30th AIAA Fluid Dynamics Conference, Norfolk, VA, AIAA 99-3588, June 28–July 1, 1999.

[6] A.D. Cutler, J.A. White, An experimental and CFD study of a supersonic coaxial jet, in: Proceedings of the 39th Aerospace Sciences Meeting, Reno, NV, AIAA Paper 2001-0143, January 8–11, 2001.

[7] A.D. Cutler, G.S. Diskin, P.M. Danehy, J.P. Drummond, Fundamental mixing and combustion experiments for propelled hypersonic flight, in: Proceedings of the 38th AIAA/ASME/SAE/ASEE Joint Propulsion Conference and Exhibit, Indianapolis, Indiana, AIAA Paper 2002-3879, July 7–10, 2002.

[8] J.P. Drummond, G.S. Diskin, A.D. Cutler, P.M. Danehy, Fuel–air mixing and combustion in scramjets, in: Proceedings of the 38th AIAA/ASME/SAE/ASEE Joint Propulsion Conference and Exhibit, Indianapolis, Indiana, AIAA Paper 2002-3878, July 7–10, 2002.

[9] A.D. Cutler, D.S. Diskin, J.P. Drummond, J.A. White, Supersonic coaxial jet experiment for computational fluid dynamics code validation, AIAA J. 44 (3) (2006) 585–592.

[10] C.W Clifton and A.D. Cutler, A Supersonic Argon/Air Coaxial Jet Experiment for Computational Fluid Dynamics Code Validation, Report No. NASA/CR-2007-214866.

[11] R.A. Baurle, J.R. Edwards, Hybrid reynolds-averaged/large-eddy simulations of a coaxial supersonic freejet experiment, AIAA J. 48 (3) (2010) 551–571.

[12] J.A. White, J.H. Morrison, A pseudo-temporal multi-grid relaxation scheme for solving the parabolized Navier–Stokes equations, AIAA Paper 99-3360, June 1999.

[13] D.C. Wilcox, Turbulence Modeling for CFD, 2nd ed. DCW Industries, La Canada, CA, 1998.

[14] ANSYS CFX, Release 11.0: Installation and Overview, July 7th 2007.

[15] S. Doehner M.S. thesis, Effects of Jet Swirl on Mixing of a Light Gas Jet in a Supersonic Airstream, The George Washington University, Washington, USA, 1999.

[16] R.B. Miles, J. Grinstead, R.H. Kohl, G.S. Diskin, The RELIEF flow tagging technique and its application in engine testing facilities and for helium–air mixing studies, Meas. Sci. Technol. 11 (2000) 1272–1281.

[17] P. Manna, Debasis Chakraborty, Numerical investigation of transverse sonic injection in a nonreacting supersonic combustor, ASME J. Aerosp. Eng. Part G 219 (3) (2005) 205–215.

[18] Malsur Dharavath, P.K. Sinha, Debasis Chakraborty, Simulation of supersonic base flow – effect of computational grid and turbulence model, ASME J. Aerosp. Eng. 224 (3) (2010) 311–319.

[19] S. Saha, S. Rathod, M.S.R Chandra Murty, P.K. Sinha, Debasis Chakraborty, Numerical simulation of base flow of a long range flight vehicle, Acta Astronaut. 74 (3) (2012) 112–119.

[20] G. Aswin, Debasis Chakraborty, Numerical simulation of transverse side jet interaction with supersonic free stream, Aerosp. Sci. Technol. J. 14 (2010) 295–301.

[21] Soumyajit Saha, Debasis Chakraborty, Hypersonic intake starting characteristics – a CFD Validation study, Def. Sci. J. 62 (3) (2012) 147–152.

[22] Malsur Dharavath, Debasis Chakraborty, Numerical simulation of supersonic jet impingement on inclined plate, Def. Sci. J. 63 (4) (2013) 355–362.

[23] P.K. Sinha and Debasis Chakraborty, Numerical study of flow inside a tube during hot launching of rocket, J. Aerosp. Eng., Vol 228, pp2604-2611, December,2014.

[24] T.J. Barth, D.C. Jesperson, The design and application of upwind scheme on unstructured meshes, AIAA paper 89-0366, 1989.

[25] B.E Launder, D.B Spalding, The numerical computation of turbulent flows, Comput. Methods Appl. Mech. Eng. 3 (1974) 269–289.

[26] F.R Menter, M. Kuntz, R. Bender, A scale adaptive simulation model for turbulent flow predictions, AIAA paper 2003-0767, 2003.

[27] Afroz Javed, Debasis Chakraborty, P.J. Paul, Model free simulation of compressible mixing layers, J. Aerosp. Eng. 227 (6) (2013) 977–999.

[28] Amid Ansari, Self-similarity and mixing characteristics of turbulent mixing layers starting from laminar initial conditions, Phys. Fluids 9 (6) (1997) 1714–1718.

[29] M.W. Plesniak, J.H. Bell, R.D. Mehta Effects of initial spanwise perturbations and three dimensionality in a plane mixing layer, AIAA paper 91-0622, 1991.